Amorphous/Crystalline Materials

DOI: 10.1002/anie.201205081

Amorphous-to-Crystalline Transformation with Fluorescence Enhancement and Switching of Molecular Nanoparticles Fixed in a Polymer Thin Film**

*Ch. G. Chandaluri and T. P. Radhakrishnan**

The classical model for crystallization visualizes the formation of a metastable crystalline nucleus that through density fluctuations reaches a critical size and grows into a stable crystal. The two-step nucleation theory invoking a liquid-like cluster intermediate developed to explain protein crystallization,[1,2] has been shown to be of more general validity, and applicable to macromolecule as well as small molecule crystals.[3] The amorphous-to-crystalline transformation (ACT) familiar in protein–mineral composites,[4–6] pharamaceuticals[7,8] and inorganics[9–15] including phase-change materials,[16] is of potential interest in the context of molecular crystals and nanocrystals as well. Heterogeneous nucleation and growth in confined environments[17] add a further dimension to the crystallization process.

The coexistence of amorphous/crystalline regions and the impact of crystallinity on properties in macromolecules are well-known. Targeted fabrication of the amorphous state, realization of the ACT and the crystallinity–property correlation in small-molecule-based materials have been explored little, but are significant from the conceptual as well as application perspectives. Thermal annealing induces such changes, for example, in rubrene[18] and methanofullerene[19] thin films. Crystalline and amorphous forms of (4-biphenylyl)phenyldibenzofulvene were interconverted by solvent vapor fuming, heating and cooling, the former exhibiting enhanced fluorescence.[20] The photosensitivity of dye aggregates increased when crystallinity was induced through solvent vapor fuming.[21] The crystallinity of materials critically affects the charge mobilities in organic light-emitting diodes (OLEDs).[22] To explore the ACT in small-molecule-based materials, it is imperative to develop a molecular design and protocol for the fabrication of amorphous particles followed by their crystallization, and monitor the transformation together with some materials response that evolves concomitantly.

Crystals of 7,7-diamino-8,8-dicyanoquinodimethanes (DADQs) exhibit strong fluorescence enhancement relative to their solutions, because of the inhibition of excited-state geometry relaxation in the former case.[23] The emission color can be tuned by structural variations[24–26] and nanocrystals with strong emission have been fabricated.[24,27] The zwitterionic DADQs crystallize easily as observed with NLO-active[28] and fluorescent[23–27] derivatives (NLO = nonlinear optical). Present explorations show that specific structural motifs promote the formation of amorphous particles, when solutions are drop-cast onto suitable substrates. As traditional methods failed to induce an ACT, we developed a novel protocol involving fuming of particles partially confined by fixing in a polymer thin film. The transformation is monitored by microscopy along with the accompanying fluorescence switching and enhancement.

DADQs bearing aromatic rings linked through conformationally labile bonds[29] are found to form amorphous particles when dilute solutions are drop-cast onto hydrophilic substrates like glass. We consider 7,7-bis(2-(4-bromophenyl)ethylamino)-8,8-dicyanoquinodimethane (BBPEDQ, Figure 1 a) synthesized by condensation of 2-(4-bromophenyl)ethylamine and 7,7,8,8-tetracyano-*p*-quinodimethane (TCNQ).[29,30] Crystals grown in methanol solution belong to the space group *Pbca*.[29,31] The crystal structure reveals

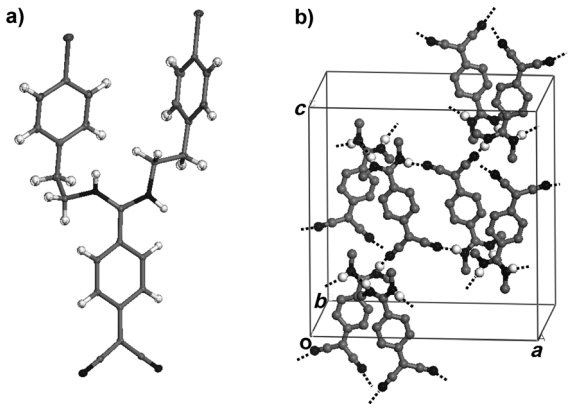

Figure 1. a) Molecular and b) crystal structure of BBPEDQ from single-crystal X-ray analysis; C (gray), H (white), N (black), Br (dark gray), intermolecular H bond (dashed line). In (b), H atoms not involved in the H bonds are omitted and only one C atom of the 2-(4-bromophenyl)ethyl group is retained for clarity.

[*] Ch. G. Chandaluri, Prof. T. P. Radhakrishnan
School of Chemistry, University of Hyderabad
Hyderabad, 500 046 (India)
E-mail: tprsc@uohyd.ernet.in

[**] Financial support from the Department of Science and Technology, New Delhi and infrastructure support from the Centre for Nanotechnology and the National Single Crystal X-ray Diffractometer Facility (School of Chemistry) at the University of Hyderabad are gratefully acknowledged. C.G.C. thanks the CSIR, New Delhi for a senior research fellowship. We thank M. Durgaprasad, M. Laxminaryana, and M. Nalini for the transmission electron microscopy, field emission scanning electron microscopy, and confocal fluorescence microscopy, respectively.

Supporting information for this article, including details of synthesis and characterization, crystal structure, spectroscopy, microscopy, and computations, is available on the WWW under http://dx.doi.org/10.1002/anie.201205081.

intermolecular amino–cyano H bonds leading to dimer motifs and extended chains (Figure 1). The optical absorption spectrum of a methanol solution of BBPEDQ has a maximum (λ_{max}) at 371 nm; the microcrystalline solid shows a broad (300–420 nm) absorption (Figure 2a). The fluorescence emission exhibits a clear peak shift from 485 nm (nearly green) in solution to 462 nm (nearly blue) in the microcrystals,[29] with the intensity increasing about 235 times (Figure 2b). The quantum yields are 0.2 and 20.0% in solution and microcrystals, respectively. Time-dependent density functional computations were carried out to study the electronic structure of BBPEDQ and its dimers. The computed lowest-energy excitation with high oscillator strength of BBPEDQ (fully optimized structure in a methanol environment) is at 385.3 nm, which is consistent with the solution spectrum. Computations on the H-bonded dimers (Figure 1b) with antiparallel and quasi-parallel dipoles (reminiscent of H and J dimers) gave the lowest-energy excitations at 368.2 nm in the antiparallel case and at 394.7, 392.3 and 377.0 nm in the quasi-parallel case.[29] This is consistent with the broad absorption of the solid; the higher excitation energy of the "H-type" dimer possibly leads to the blue shift of the emission.

Drop-casting a methanol solution of BBPEDQ onto glass followed by slow evaporation in ambient atmosphere and vacuum drying produced a thin film of hemispherical particles of a uniform size. The particle size can be tuned from about 700 to 50 nm by varying the solution concentration from 1.00 to 0.01 mM (Figure 3). Interesting morphologies like network structures can be realized by changing the solvent and the substrate.[29] Optical spectra of the films on quartz are shown in Figure 2c and d; the λ_{max} of the absorption and emission are at 390 and 487 nm, respectively. The films produce a green emission on illumination by a UV (365 nm) lamp. A comparison with the solution and microcrystals suggests that these particles, even though solid, are far from crystalline. The hydrophobic substituents on BBPEDQ promote dewetting on a glass substrate, and the conformational lability of the molecule leads to an amorphous assembly.

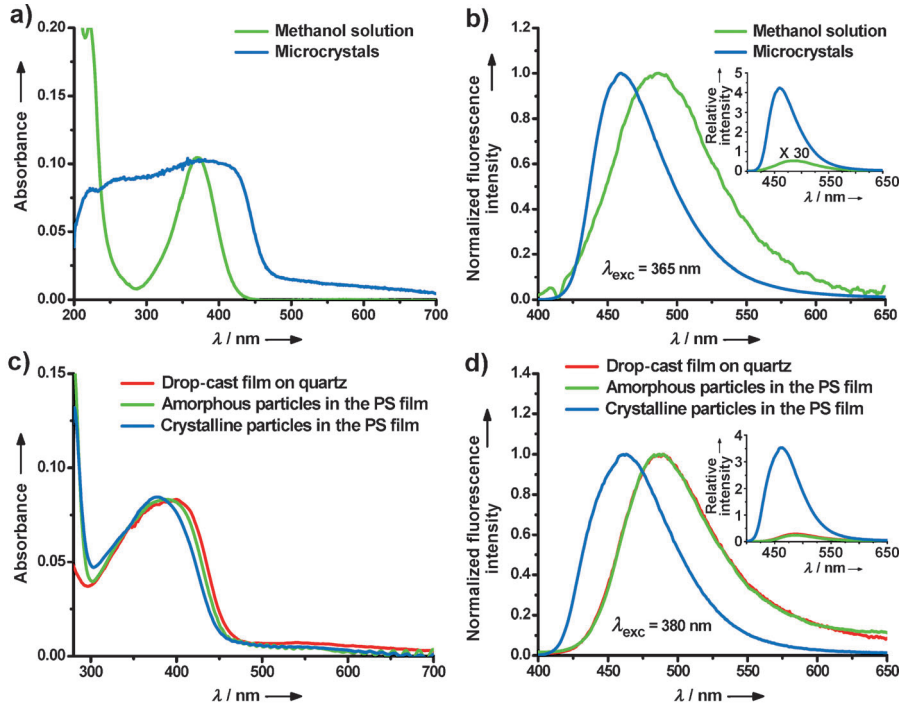

Figure 2. Optical spectra of BBPEDQ. a) Absorption spectra of microcrystals and methanol solution (concentration adjusted to match peak absorbance). b) Normalized fluorescence emission spectra of microcrystals and methanol solution (inset: spectra of samples with matched absorbances). c,d) The corresponding spectra of a drop-cast film on quartz and a free-standing PS film with nanoparticles before (amorphous) and after 5 min of exposure to methanol vapor (crystalline). Excitation wavelengths for the emission spectra are indicated.

Common techniques like heating and exposure to solvent fumes used to induce crystallization of amorphous particles led to the aggregation of BBPEDQ particles,[29] but not to crystallization. This prompted us to develop a new protocol for confining the particles before attempting the ACT (Figure 4). A toluene solution of polystyrene (PS) was spin-coated on top of the drop-cast film on glass and dried under vacuum; it was then peeled off to give a free-standing film. Images of the lower side of the film show the circular particles fixed there (Figure 5a). This side was then exposed to methanol vapor for short periods of time. Images of the film (Figure 5b–d) demonstrate the formation of faceted particles and their

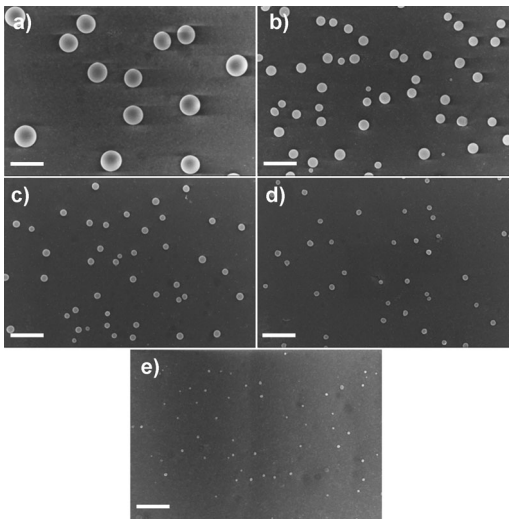

Figure 3. FESEM images of BBPEDQ nanoparticles obtained by drop-casting methanol solutions of different concentrations. a) 1, b) 0.5, c) 0.1, d) 0.05, and e) 0.01 mM on a glass substrate; scale bars = 1 μm.

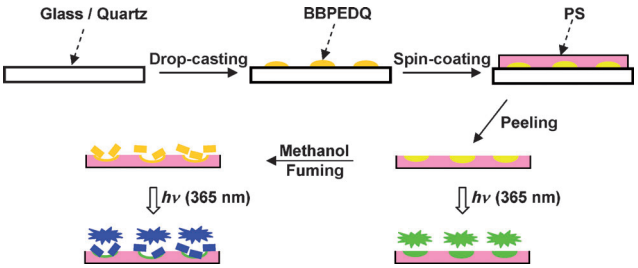

Figure 4. Protocol for drop-casting, fixing in a PS film and solvent vapor fuming to induce an amorphous-to-crystalline transformation. Fluorescence responses of the crystalline and amorphous nanoparticles are indicated schematically.

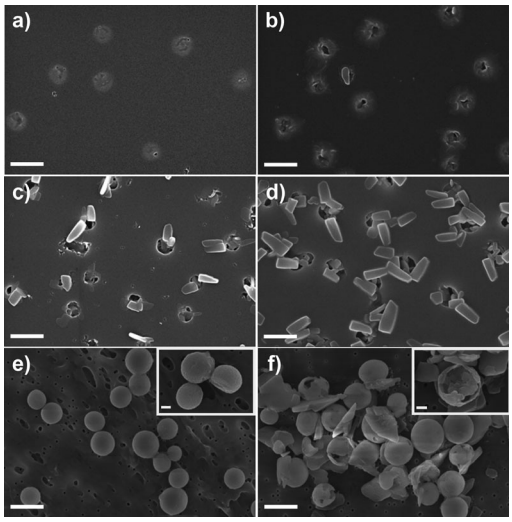

Figure 5. FESEM images of BBPEDQ nanoparticles. a) Fixed in a PS film. b–d) Fixed in a PS film and exposed to methanol vapor for 1, 3, and 5 min. e, f) Obtained by dissolving the PS films shown in (a) and (d) in toluene and filtering through nanoporous polycarbonate membrane; scale bars = 1 μm. In the insets in (e) and (f) the morphology of particles is highlighted; scale bars = 200 nm.

emergence from the circular slots in the polymer, in which the amorphous particles were hosted, a case of square peg in a round hole. On exposure of the film to methanol vapor, the optical absorption shifts slightly (Figure 2c), but the emission peak shows a definitive blue-shift from 487 to 462 nm (Figure 2d), in a manner identical to that of solution and microcrystals. The fluorescence shift is clearly indicative of an ACT. The fluorescence intensity increases about 13 times upon crystallization; quantum yields are 7.3 and 15.4% in the amorphous and crystalline forms, respectively. TEM images of the particles freed by dissolving the PS in toluene were recorded.[29] While the circular particles showed no electron diffraction spots (Figure 6a), the faceted particles obtained by exposure to methanol showed a diffraction pattern (Figure 6b) consistent with the crystal structure of BBPEDQ,[29] proving the formation of nanocrystals unambiguously. There was no definitive evidence of the ACT under electron beam irradiation, even though such a possibility exists. Confocal fluorescence images were recorded using emission in the 410–430 and 620–650 nm windows, excluding the emission from

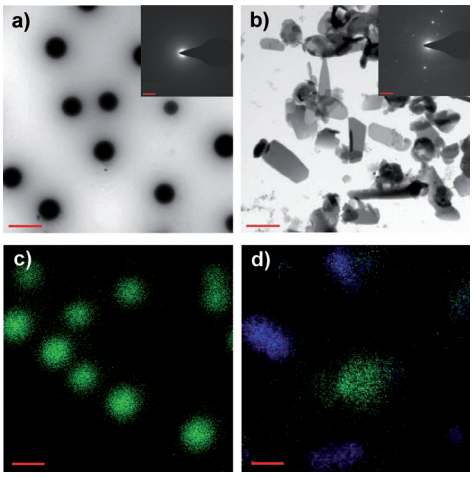

Figure 6. TEM images and selected-area electron diffraction (inset, scale bar = 2 1/nm) of BBPEDQ nanoparticles in a PS film a) before and b) after exposure to methanol vapor. Laser scanning confocal fluorescence images of the film c) before and d) after exposure to methanol vapor; blue and green colors represent emission in the 410–430 and 620–650 nm windows, respectively; scale bars in (a-d) = 1 μm.

the amorphous and crystalline particles, respectively (Figure 2d); these are colored blue and green in Figure 6c,d. The film before exposure to methanol shows the emission from amorphous particles alone. Emissions from the coexisting crystalline (elongated) and amorphous (circular) particles in the exposed film are shown superposed in Figure 6d.[29]

The amorphous and crystalline nanoparticles were isolated by dissolving the PS films in toluene, filtering through a nanoporous membrane, and washing with toluene to remove any remnant PS. Particles from the film before exposure to methanol are hemispherical domes as expected (Figure 5e). Interestingly, those from the exposed film show hemispherical shells with nanocrystals inside and outside (Figure 5f). The images suggest the following mechanism of ACT. Methanol vapor condenses on the amorphous particles fixed in the PS film forming a liquid-like cluster inside the cavities. Crystalline nuclei emerging within this cluster as visualized in the two-step nucleation model grow into stable nanocrystals. The molecules in contact with the cavity wall, possibly involved in hydrophobic interactions with the polymer, stay in amorphous state forming the shell.

The present study provides significant insight into the nucleation and growth of molecular nanocrystals. Molecular features and substrate characteristics conducive to the formation of amorphous particles in drop-cast films are identified. The protocol involving solvent vapor fuming of amorphous particles fixed in polymer cavities provides a facile route to the ACT abd its demonstration. The enhanced and shifting fluorescence emission accompanying the ACT makes BBPEDQ of considerable interest as novel materials.

Received: June 28, 2012
Published online: October 17, 2012

Keywords: amorphous materials · fluorescence · nanoparticles · polymers · thin films

[1] P. G. Vekilov, *J. Cryst. Growth* **2005**, *275*, 65 – 76.
[2] P. G. Vekilov, *Nanoscale* **2010**, *2*, 2346 – 2357.
[3] D. Erdemir, A. Y. Lee, A. S. Myerson, *Acc. Chem. Res.* **2009**, *42*, 621 – 629.
[4] X. Cheng, L. B. Gower, *Biotechnol. Prog.* **2006**, *22*, 141 – 149.
[5] C. Wu, J. Martel, D. Young, J. D. Young, *PloS ONE* **2009**, *4*, e8058.
[6] H. Peng, J. Martel, Y. Lee, D. M. Ojcius, J. D. Young, *Nanomedicine* **2011**, *6*, 643 – 658.
[7] S. Strydom, W. Liebenberg, L. Yu, M. de Villiers, *Int. J. Pharm.* **2009**, *379*, 72 – 81.
[8] D. Xia, J. X. Wu, F. Cui, H. Qu, T. Rades, J. Rantanen, M. Yang, *Eur. J. Pharm. Sci.* **2012**, *46*, 446 – 454.
[9] S. Hasegawa, S. Horike, R. Matsuda, S. Furukawa, K. Mochizuki, Y. Kinoshita, S. Kitagawa, *J. Am. Chem. Soc.* **2007**, *129*, 2607 – 2614.
[10] Y. Jeon, J. Heo, C. A. Mirkin, *J. Am. Chem. Soc.* **2007**, *129*, 7480 – 7481.
[11] J. Tao, H. Pan, H. Zhai, J. Wang, L. Li, J. Wu, W. Jiang, X. Xu, R. Tang, *Cryst. Growth Des.* **2009**, *9*, 3154 – 3160.
[12] V. B. Mortola, A. P. Ferreira, J. M. Fedeyko, C. Downing, J. M. C. Bueno, M. C. Kung, H. H. Kung, *J. Mater. Chem.* **2010**, *20*, 7517 – 7525.
[13] L. C. Jacobson, V. Molinero, *J. Am. Chem. Soc.* **2011**, *133*, 6458 – 6463.
[14] S. Jana, R. M. Rioux, *Nanoscale* **2012**, *4*, 1782 – 1788.
[15] J. Xiao, S. Yang, *Nanoscale* **2012**, *4*, 54 – 65.
[16] S. Raoux, D. Ielmini, M. Wuttig, I. Karpov, *MRS Bull.* **2012**, *37*, 118 – 123.
[17] B. D. Hamilton, J. Ha, M. A. Hillmyer, M. D. Ward, *Acc. Chem. Res.* **2012**, *45*, 414 – 423.
[18] S. Park, J. Choi, K. H. Lee, H. W. Yeom, S. Im, Y. K. Lee, *J. Phys. Chem. B* **2010**, *114*, 5661 – 5665.
[19] L. Zheng, J. Liu, Y. Ding, Y. Han, *J. Phys. Chem. B* **2011**, *115*, 8071 – 8077.
[20] Y. Dong, J. W. Y. Lam, A. Qin, Z. Li, J. Sun, H. H.-Y. Sung, I. D. Williams, B. Z. Tang, *Chem. Commun.* **2007**, 40 – 42.
[21] B. Z. Tang, H. Z. Chen, R. S. Xu, J. W. Y. Lam, K. K. L. Cheuk, H. N. C. Wong, M. Wang, *Chem. Mater.* **2000**, *12*, 213 – 221.
[22] Y. Shirota, H. Kageyama, *Chem. Rev.* **2007**, *107*, 953 – 1010.
[23] S. Jayanty, T. P. Radhakrishnan, *Chem. Eur. J.* **2004**, *10*, 791 – 797.
[24] A. Patra, N. Hebalkar, B. Sreedhar, M. Sarkar, A. Samanta, T. P. Radhakrishnan, *Small* **2006**, *2*, 650 – 659.
[25] C. G. Chandaluri, T. P. Radhakrishnan, *Opt. Mater.* **2011**, *34*, 119 – 125.
[26] A. Patra, T. P. Radhakrishnan, *Chem. Eur. J.* **2009**, *15*, 2792 – 2800.
[27] C. G. Chandaluri, A. Patra, T. P. Radhakrishnan, *Chem. Eur. J.* **2010**, *16*, 8699 – 8706.
[28] T. P. Radhakrishnan, *Acc. Chem. Res.* **2008**, *41*, 367 – 376.
[29] See the Supporting Information.
[30] W. R. Hertler, H. D. Hartzler, D. S. Acker, R. E. Benson, *J. Am. Chem. Soc.* **1962**, *84*, 3387 – 3393.
[31] Crystallographic data: Orthorhombic *Pbca*, $a = 18.7191(17)$, $b = 13.4503(12)$, $c = 19.2747(17)$ Å, $V = 4852.9(8)$ Å^3, $\rho_{calcd} = 1.506\ g\,cm^{-3}$, $T = 100$ K, number of measured reflections = 4289, number of parameters = 297, $R = 0.0315$, $wR^2 = 0.0801$, largest difference peak, hole = 0.481, $-0.731\ e\,Å^{-3}$; CCDC 887747 contains the supplementary crystallographic data for this paper. These data can be obtained free of charge from The Cambridge Crystallographic Data Centre via www.ccdc.cam.ac.uk/data_request/cif.

